catalysts

MDPI

Article

Hydrogen Production from Chemical Looping Steam Reforming of Ethanol over Perovskite-Type Oxygen Carriers with Bimetallic Co and Ni B-Site Substitution

Lin Li, Bo Jiang, Zhehao Sun, Qian Zhang, Duyu Li and Dawei Tang *

Key Laboratory of Ocean Energy Utilization and Energy Conservation of Ministry of Education, Dalian University of Technology, Dalian 116024, China; lilinnd@dlut.edu.cn (L.L.); ericchiang@mail.dlut.edu.cn (B.J.); sunzhehao@mail.dlut.edu.cn (Z.S.); zhangqianqian@mail.dlut.edu.cn (Q.Z.); duyuli0921@gmail.com (D.L.)

* Correspondence: dwtang@dlut.edu.cn; Tel.: +86-0411-8470-8460

Received: 13 August 2018; Accepted: 29 August 2018; Published: 4 September 2018

Abstract: This paper describes the synthesis of a series of $La_{1.4}Sr_{0.6}Ni_{1-x}Co_xO_4$ perovskite OCs using co-precipitation method by employing Co and Ni as the B-site components of perovskite and the synergetic effect of Co doping on chemical looping reforming of ethanol. A variety of techniques including N_2 adsorption-desorption, X-ray diffraction (XRD), transmission electron microscopy (TEM) and H_2 temperature-programmed reduction (TPR) were employed to investigate the physicochemical properties of the fresh and used OCs. The activity and stability in chemical looping reforming were studied in a fixed bed reactor at 600 °C and a S/C ratio of three. The synergetic effect between Ni and Co was able to enhance the catalytic activity and improve the stability of perovskite OCs. $La_{1.4}Sr_{0.6}Ni_{0.6}Co_{0.4}O_4$ showed an average ethanol conversion of 92.4% and an average CO_2/CO ratio of 5.4 in a 30-cycle stability test. Significantly, the H_2 yield and purity reached 11 wt.% and 73%, respectively. The Co doping was able to significantly improve the self-regeneration capability due to the increase in the number of oxygen vacancies in the perovskite lattice, thereby enhancing the sintering resistance. Moreover, Co promotion also contributes to the improved WGS activity.

Keywords: chemical looping reforming; perovskite; Ni-Co synergy

1. Introduction

Hydrogen is an environmentally benign fuel source which mitigates the global dependency on fossil fuels [1,2]. Chemical looping steam reforming (CLSR) is a novel hydrogen production technology which significantly differs from conventional steam reforming and other hydrogen production technologies. As illustrated in Figure 1, the oxygen carriers (OCs) were circulated between a fuel feed stage and an air feed stage in a CLSR process. The oxidation reaction in the air feed stage is exothermic, and the generated heat can be supplied for the following fuel feed reaction that converts fuel into hydrogen, thus reducing the energy consumption (Table 1) [3]. Meanwhile, carbon deposition formed on the OCs can be eliminated during the air feed step. These advantages of CLSR enable it to be an economical and efficient approach for hydrogen production.

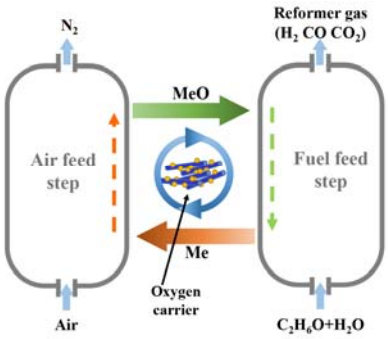

Figure 1. Schematic diagram of chemical looping process.

Table 1. Reactions during fuel feed step and air feed step.

Step	Reactions
Fuel Feed Step	$C_2H_5OH + H_2O \xrightarrow{Ni} 2CO + 4H_2$
	$CO + H_2O \rightarrow CO_2 + H_2$
	$C_2H_5OH + 6NiO \rightarrow 6Ni + 2CO_2 + 3H_2O$
Air Feed Step	$C + O_2 \rightarrow CO_2$
	$2C + O_2 \rightarrow 2CO$
	$2Ni + O_2 \rightarrow 2NiO$

The selection of high-performance OCs is a key issue for CLSR. Among various metal oxides, Ni-based OCs have attracted much attention due to their strong ability to rupture C–C bonds, excellent redox property and low cost. However, its application is still limited by the severe coke deposition and metal sintering. Many previous investigations have committed to solving the deactivation of OCs [4,5]. Single component metal nanoparticles are easy to agglomerate at high temperature, thus leading to severe active phase sintering. The redox property and mobility of metal nanoparticles could be modified by doping another metal, and the synergistic effect between two different metals would affect the catalytic activity of OCs [6]. According to this principle, some bimetallic OCs have been prepared and investigated in steam reforming, such as Ni-Fe, Cu-Co, Cu-Ni and Co-Ni [7]. The Cu-Co and Cu-Ni-based OCs exhibit high hydrogen selectivity and ethanol conversion, but show poor stability after multi-cycle reaction. In comparison, Ni-Co-based OCs show higher stability, which is due to the strong interaction between Co and Ni. Another efficient way to improve sintering resistance is to accommodate the Ni nanoparticles in unique-structure supports such as hydrotalcite, perovskite and montmorillonite [1,8–10]. Nowadays, perovskite-type metal oxides as OCs with a general formula of ABO_3 or A_2BO_4 have been drawing much attention. Such structures are easy to interact with transition metals, which is beneficial to improve the dispersion of active component. The most significant property of perovskite is its self-regeneration ability in CLSR process [11]. At the fuel feed stage, the perovskite would be reduced, and the active metal nanoparticles could generate from the perovskite lattice, which is responsible for the catalytic reaction. At the subsequent air feed stage, the active metal would be reversibly oxidized into the perovskite lattice, and the OC could be regenerated. The structural transformation of perovskite may inhibit the growth of metal particles [12]. Additionally, the lattice distortion in perovskite would generate a large number of oxygen vacancies which can oxidize the formed carbon, thus improving the resistance to coke deposition [13].

The structural and self-regeneration characteristics of perovskite could be regulated via partially substituting A or B sites components. Various types of A and B cations in perovskite structure have been studied. Kawi et al. [14] discovered that the Ni^{3+} in $LaNiO_3$ could be readily reduced to Ni and distributed on La_2O_3 support. Morales et al. [15] studied the $La_{0.6}Sr_{0.4}CoO_{3-d}$ perovskite for ethanol steam reforming and have observed the movement of metallic cobalt from perovskite lattice to the

surface of OCs. Wu et al. [16] developed a series of $La_{1-x}Ca_xNiO_3$ catalysts for hydrogen production by glycerol steam reforming. Ni and Co are commonly used as active B-site metals in perovskite OCs. However, as a single metal component, Ni or Co still suffers from severe metal sintering when it is generated from the perovskite [11]. As mentioned above, the bimetallic structure perovskite can enhance the interaction of two metals, thus improving the dispersion of metal nanoparticles and suppressing metal sintering [17–19].

In this work, we propose a novel type of $La_{1.4}Sr_{0.6}Ni_{1-x}Co_xO_4$ perovskite OC for hydrogen production by employing Co and Ni as the B-site components of perovskite. The synergistic effect between Ni and Co is conducive to the enhancement of the catalytic activity and the stability of perovskite OCs. The $La_{1.4}Sr_{0.6}Ni_{1-x}Co_xO_4$ OCs are prepared by a coprecipitation method and are characterized by X-ray diffraction (XRD), transmission electron microscopy (TEM), H_2 temperature-programmed reduction (H_2-TPR) and inductively coupled plasma optical emission spectroscopy (ICP-OES). The reactivity and stability of the proposed OCs are performed in a fixed-bed reactor.

2. Results and Discussion

2.1. Characterization of OCs

The physical properties of fresh OCs are listed in Table 2. The BET areas of these prepared OCs are lower than 10 m^2/g, which is consistent with the inherent characteristics of perovskite-type structures. The Ni or Ni-Co alloy particle sizes after reduction were calculated from the (111) plane at 44.7°. The particle sizes decreased in the following sequence: $La_{1.4}Sr_{0.6}NiO_4$ (14.5 nm) > $La_{1.4}Sr_{0.6}Ni_{0.6}Co_{0.4}O_4$ (13.7 nm) > $La_{1.4}Sr_{0.6}Ni_{0.2}Co_{0.8}O_4$ (12.8 nm).

Table 2. Physical properties of oxygen carriers.

Sample	Surface Area (m^2/g)	Average Pore Diameter (nm)	Pore Volume (cm^3/g)	Ni Content [a] (wt.%)	Co Content [a] (wt.%)	Ni crystal Size after Reduction [b] (nm)
$La_{1.4}Sr_{0.6}NiO_4$	5.3	40.3	0.02	16.87	0	14.5
$La_{1.4}Sr_{0.6}Ni_{0.6}Co_{0.4}O_4$	6.1	44.1	0.03	10.32	5.99	13.7
$La_{1.4}Sr_{0.6}Ni_{0.2}Co_{0.8}O_4$	6.7	41.9	0.03	4.26	11.14	12.8

[a] Determined by ICP-OES. [b] Determined by the Scherrer's equation from (111) planes at 44.7°.

Figure 2a illustrates the XRD profiles of the fresh OCs. All samples possessed clear perovskite diffraction peaks and no obvious NiO and Co_3O_4 peaks were detected, indicating that pure perovskite-type OCs had been formed. The diffraction peaks of perovskite shifted to a higher angle with the doping of cobalt at B site. This is because that the radius of Ni^{3+} ion is larger than that of Co^{3+}. The substitution of Co^{3+} results in decreases in the crystal size and *d* spacing, therefore shifting the 2θ to a higher degree [20]. Zhao et al. [21] also observed that the main diffraction peaks of the perovskite phase shift to a higher 2θ value when cobalt ions are doped into the B site. The shift of diffraction angles suggests that cobalt and nickel are both incorporated into the perovskite lattice. The XRD profiles of the reduced OCs are exhibited in Figure 2b. After reduction, the perovskite structure disappeared, and the active component in perovskite is transformed into the metal phase before it migrates out of the perovskite lattice. The SrO_2 and La_2O_3 also formed, accompanying the decomposition of the perovskite structure. Table 3 lists the *d* spacings and diffraction angles of the Ni particles formed from the reduction of $La_{1.4}Sr_{0.6}Ni_{1-x}Co_xO_4$ OCs. The diffraction peaks of Ni (111) and Co (111) are located at 44.7° and 44.2°, respectively. The *d* spacing of Ni (111) increased with the amount of Co. Moreover, the diffraction angles also shift between Ni (111) and Co (111). The above results indicate Ni and Co are reduced from the OCs in the state of solid solution. The particle sizes calculated from the (111) plane are shown in Table 2, which are about 10 nm for all the samples. The weak peaks of La_2O_3 are shown in the diffraction profiles of reduced OCs, which are derived from the

reduction of Co and Ni. With the reduction of Ni^{3+} and Co^{3+}, the La_2O_3 would be uniformly mixed with the Ni-Co alloy. It has been demonstrated that the La promotion could significantly improve the sintering resistance and coke resistance in steam reforming process [10,22]. The XRD patterns of the reduced OCs also displayed evident diffraction peaks of $La_2O_2CO_3$, which are possibly generated via the reaction of La_2O_3 and CO_2 [22].

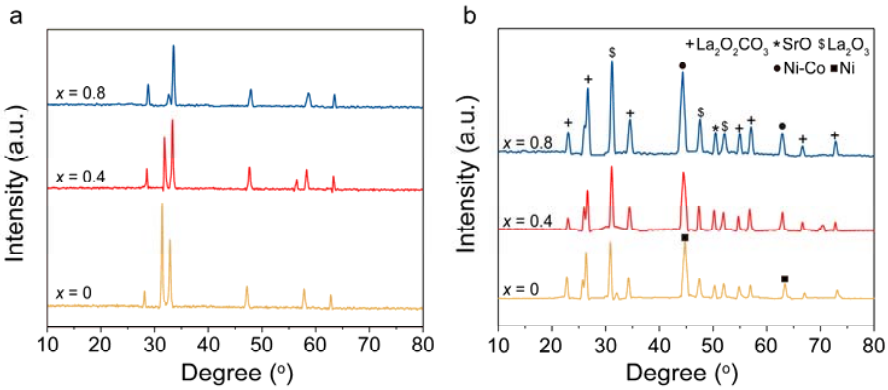

Figure 2. XRD profiles of (**a**) fresh oxygen carriers and (**b**) reduced oxygen carriers.

Table 3. Relationship between oxygen carrier and *d* spacings of Ni or Ni-Co alloy (111) planes at 2θ = 44.20°–44.70° after reduction.

Metal Particle	Ni (111)	$Co_{0.4}$-Ni	$Co_{0.8}$-Ni	Co (111)
d spacing/Å	2.026	2.031	2.050	2.052
2θ/°	44.7	44.6	44.5	44.2

The TEM images of $La_{1.4}Sr_{0.6}Ni_{0.4}Co_{0.6}O_4$ after reduction are shown in Figure 3. The Ni-Co particles with lattice stripes after the reduction were observed. Clear lattice stripes of the alloy appeared after the region was enlarged, and the interstitial void of which is 0.203 nm. The *d* spacing is between Ni (111) and Co (111), which indicates that the alloy is formed after the reduction of the Co-doped OCs. No apparent change was observed in terms of *d* spacing after reduction, suggesting Ni-Co alloy is very stable after reaction. The Ni-Co alloy particles were highly dispersed with the particle sizes of approximately 12 nm, which is consistent with the XRD results.

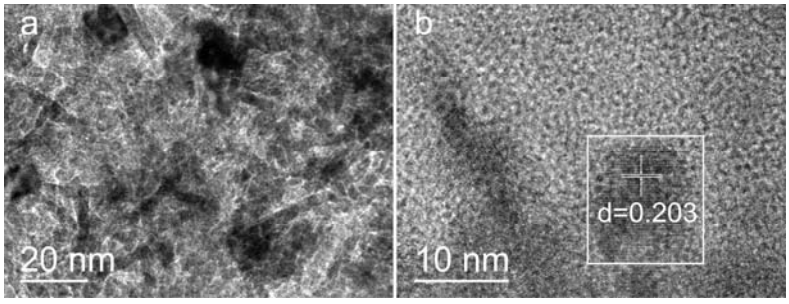

Figure 3. TEM profiles of reduced oxygen carriers.

The H_2-TPR patterns of $La_{1.4}Sr_{0.6}Ni_{1-x}Co_xO_4$ OCs are shown in of Figure 4. Generally, the valence of B site in an A_2BO_4 type perovskite is supposed to be 2+, while partial introduction of Sr^{2+} in place of La^{3+} forms unusual Co^{3+} or Ni^{3+} in these compounds [23,24]. The reduction process should be divided into two steps, i.e., from 3+ to 2+ and then from 2+ to 0. Moreover, the reduction temperature ranges of Ni and Co are close to each other [25]. Therefore, all the OCs obviously

exhibited two broad reduction peaks at 300 °C~450 °C (LT, low temperature) and 500 °C~600 °C (HT, high temperature). The peaks at HT are attributed to the reduction of Ni^{2+} or Co^{2+} to Ni^0 or Co^0, respectively. The Ni and Co metals peaks at HT merged into one reduction peak, indicating that Ni-Co alloy is formed [21]. The peaks at LT are ascribed to the reduction of Ni^{3+} or Co^{3+} to Ni^{2+} or Co^{2+}, respectively. The splitting of the LT peaks was observed for the Co doped perovskite samples. This could be due to the formation of the spinel type structure, such as $SrLaCoO_4$, promoted by the presence of Sr when the molar ratio of La to Sr is lower than five in perovskite structure [26]. The spinel phase was not detected by XRD analysis, and this is probably due to its small particle size. Moreover, the reduction peaks of LT and HT tend to move towards lower temperatures with the amount of Co, which may be due to the small particle size of perovskite particles [21]. Smaller particles could provide a higher specific surface area (listed in Table 2) and higher specific surface energy, thus lowering the reduction temperature [27]. Additionally, Valderrama et al. [28] demonstrated that Co substitution in $La_{0.8}Sr_{0.2}Ni_{1-y}Co_yO_3$ perovskite could promote the formation of positive holes and vacancies of lattice oxygen, therefore favoring the reduction process. It can be concluded that an appropriate amount doping of Co can enhance the reducibility of active components in the perovskite, thus improving the catalytic activity in a CLSR process.

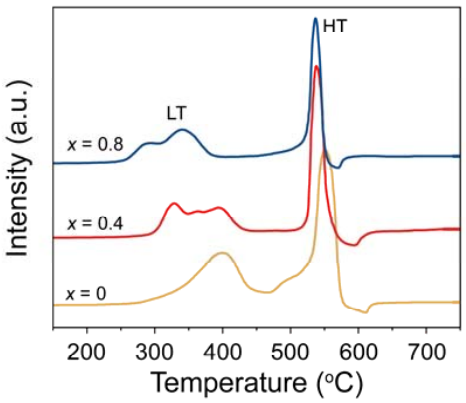

Figure 4. TPR of fresh oxygen carriers.

2.2. Activity Tests of OCs

Figure 5 displays the gas product distribution of the $La_{1.4}Sr_{0.6}Ni_{1-x}Co_xO_4$ OCs during CLSR. The hydrogen concentrations of all the three OCs increased dramatically within the first five minutes in the fuel feed step. The duration where no hydrogen is produced is known as 'dead time'. It is considered to be an important indicator of OCs' redox properties [19]. In this period, H_2 concentration was almost zero. Only when the Ni ions in the perovskite lattice are sufficiently reduced to metallic Ni can steam reforming of ethanol and subsequent in situ water gas shift (WGS) occur [29,30]. In this stage, the perovskite is gradually reduced, therefore generating the active Ni-Co alloy component. Afterwards, the reforming reaction of ethanol and WGS begins to play the dominated role in the steady stage of the fuel feed step, thus leading to a great rise in H_2 concentration in seconds. Compared with the $La_{1.4}Sr_{0.6}NiO_4$, the Co doping samples showed shorter dead time due to the improved reducibility, corresponding with the TPR results. De Lasa et al. [31] investigated the reactivity and stability of Co-Ni/Al_2O_3 OC in multicycle CLC process, and they have concluded that the Co promotion improved the reducibility of OC by affecting the metal support interaction (MSI). The average H_2 concentration of $La_{1.4}Sr_{0.6}Ni_{0.6}Co_{0.4}O_4$ OC is 17.1%, which is much higher than that of $La_{1.4}Sr_{0.6}NiO_4$ (14.3%) and $La_{1.4}Sr_{0.6}Ni_{0.2}Co_{0.8}O_4$ (12.3%). The Co doping samples showed higher CO_2 concentration and lower CO concentration than counterparts of $La_{1.4}Sr_{0.6}NiO_4$, indicating the enhanced WGS reactivity. Both Ni and Co are active for steam reforming of ethanol; however, the $La_{1.4}Sr_{0.6}Ni_{0.6}Co_{0.4}O_4$ showed superior performance in terms of H_2 and CO_2 concentrations. It is widely accepted that an effective catalyst for

steam reforming of oxygenate compounds should not only be active in cleavage of C–C bond but also be active in WGS to remove CO formed on metal surface [32]. Sinfelt et al. [33] demonstrated that Ni possesses faster rate of C–C bond rupture compared with other VIII group metals. Nevertheless, Ni has limited reactivity for WGS reaction, while Co possesses higher activity during the reaction [34]. Furthermore, Co showed high dehydrogenation activity, Ni is conducive to C–C cleavage. Thus, ethanol molecule is dehydrogenated on Co site of Ni-Co alloy, and the C–C bond is subsequently broken by the Ni site of Ni-Co alloy. This reaction route is fast, since the cleavage of the C–C bond in acetaldehyde is easier than that in ethanol molecule. Hence, $La_{1.4}Sr_{0.6}Ni_{0.6}Co_{0.4}O_4$ possesses improved capability of C–C rupture and moderate WGS activity due to the synergistic effect, therefore showing the highest H_2 concentration among three samples. Methanation is highly undesirable since it decreases H_2 yield. In our test conditions, the methane concentration is very low for all the samples, considering the strong extremely exothermic nature of methanation reaction. The Co doping samples showed high methane concentration in contrast with $La_{1.4}Sr_{0.6}NiO_4$. This is because Co is more active in methanation reactions than Ni [34].

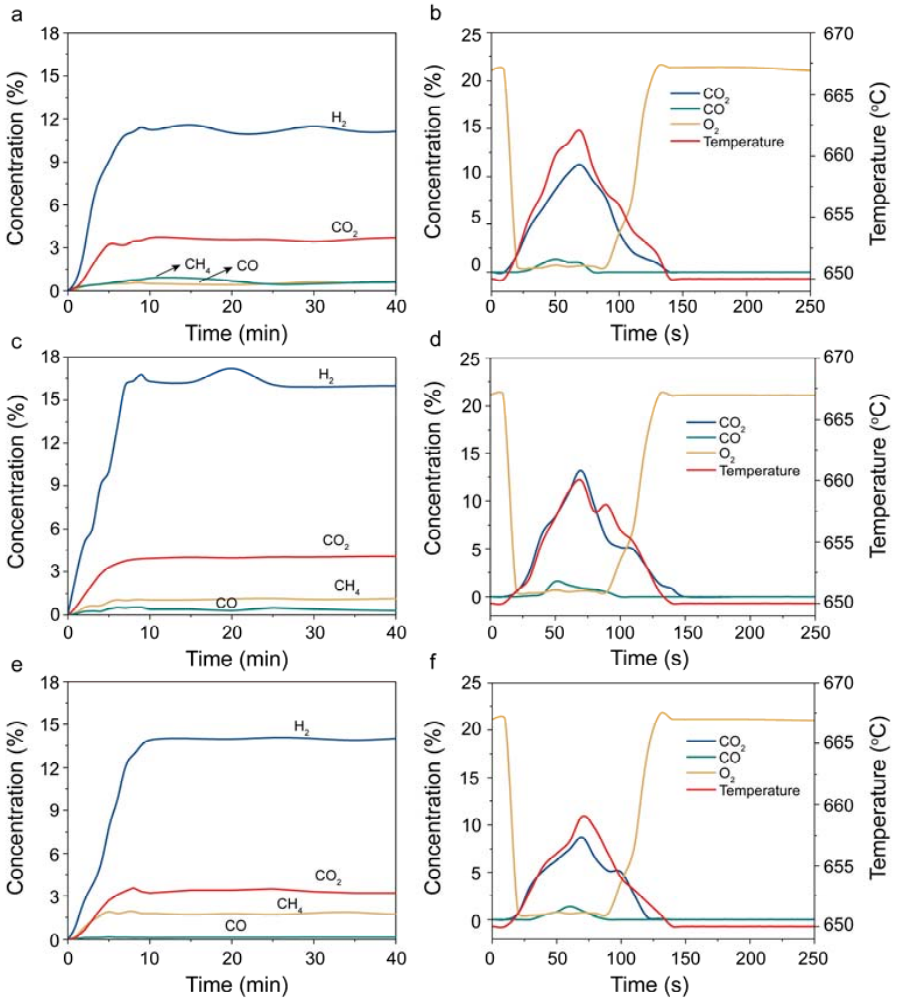

Figure 5. Activity tests in fuel feed step and air feed step. (**a**,**b**) $La_{1.4}Sr_{0.6}Ni_{0.2}Co_{0.8}O_4$; (**c**,**d**) $La_{1.4}Sr_{0.6}Ni_{0.6}Co_{0.4}O_4$; (**e**,**f**) $La_{1.4}Sr_{0.6}NiO_4$.

The gas product concentrations in the air feed step are illustrated in Figure 5. The air feed step plays three roles in a CLSR process using perovskite type OCs. Apart from providing heat and eliminating coke deposition as in a conventional CLSR process, the air feed step would also regenerate the perovskite structure [35]. It has been reported that Ni ions in the perovskite lattice

would come out of the bulk in the fuel feed step and immerse back into the lattice in the air feed step [11], therefore suppressing the growth of Ni particles and maintaining its dispersion. The peak areas of C-containing gas products represent the coke deposition amounts. The coke deposition of the three samples decreased in the following sequence: $La_{1.4}Sr_{0.6}NiO_4$ > $La_{1.4}Sr_{0.6}Ni_{0.2}Co_{0.8}O_4$ > $La_{1.4}Sr_{0.6}Ni_{0.6}Co_{0.4}O_4$, which is consistent with the order of Ni-Co alloy particle sizes listed in Table 2. It has been reported that small-sized Ni particles would increase the saturation concentration of coke deposition, which leads to a low driving force for coke diffusion over the active phase [36]. The temperature variation in the air feed step correlates with the heat release of Ni and Co oxidation and coke combustion. The end of the air feed step is signaled by the restoration of O_2 concentration to 21%.

Figure 6 shows the ethanol conversion and steam conversion of the $La_{1.4}Sr_{0.6}Ni_{1-x}Co_xO_4$ OCs during the fuel feed stage. For all the perovskite OCs, the conversion of ethanol reached at least 78%, while the conversion of steam was above 25%. The ethanol conversion of $La_{1.4}Sr_{0.6}NiO_4$ was the lowest one among three samples, while the ethanol conversion of $La_{1.4}Sr_{0.6}Ni_{0.6}Co_{0.4}O_4$ OC reached almost 100% in the first six minutes and then leveled off. When further increasing the molar ratio of Co to 0.8, the ethanol conversion dropped to 95%, resulting from the insufficiency of Ni active centers for C–C cleavage. Additionally, with the increase of Co ratio, the steam conversion also increased. Mei et al. [37] calculated water adsorption and dissociation on the Rh (111), Ni (111) and Co (0001) surfaces using Density functional theory (DFT), and their results show that water dissociation into hydroxyl and hydrogen atom on Co (0001) surface is both thermodynamically and kinetically feasible.

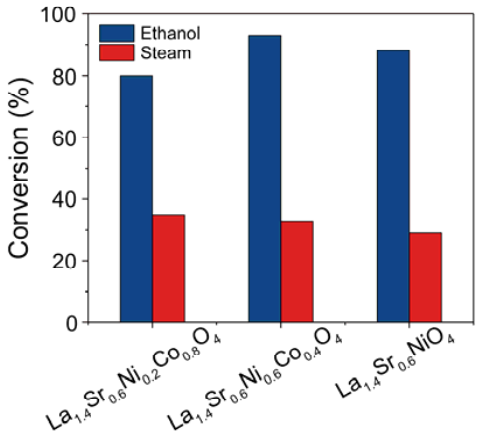

Figure 6. Ethanol and steam conversion in the fuel feed step.

2.3. Stability Tests

Figure 7 shows the variation of ethanol conversion, CO_2/CO ratio and H_2 concentration of $La_{1.4}Sr_{0.6}Ni_{1-x}Co_xO_4$ OCs during multicycle tests at 650 °C. All OCs showed decreases in ethanol conversion as well as CO_2/CO ratio after stability tests, while Co doping samples possessed more moderate variation than $La_{1.4}Co_{0.6}NiO_4$. The H_2 concentration of $La_{1.4}Sr_{0.6}Ni_{0.6}Co_{0.4}O_4$ showed an inconspicuous decrease of 0.3% at the end of the stability test, while the $La_{1.4}Sr_{0.6}NiO_4$ and $La_{1.4}Sr_{0.6}Ni_{0.2}Co_{0.8}O_4$ declined to 10.8% and 11.3%, respectively. Since the CO_2/CO ratio has been considered as an indicator for WGS activity, the decrease in the ratio is associated with the loss of the synergistic effect of the Ni-Co alloy. It has been reported that the main obstacle for Ni-based OCs is coke deposition and metal sintering [7]. Since the coke deposition can be eliminated in the air feed step, the OC deactivation in this work is mainly caused by metal sintering. As Ni is the active center for C–C bond cleavage, the decrease of ethanol conversion reflects the loss of active sites due to sintering. According to our previous investigation, the periodical movement of Ni into and out of the perovskite lattice (self-regeneration capability) could regenerate the OCs, thus improving the Ni sintering resistance [11]. Indeed, all OCs in our present work exhibited high stability, and Co doping

samples further improved the performance in stability tests. The promotion of the self-regeneration effect caused by Co doping could be explained as follows. Co substitution in $La_{0.8}Sr_{0.2}Ni_{1-y}Co_yO_3$ perovskite could promote the formation of bulk and surface defects, such as oxygen vacancies and threading dislocations, due to the radii difference between Ni and Co [28]. Surface defects, especially oxygen vacancies, could anchor Ni particles either by sharing oxygen atoms to form chemical bonds or by supplying valley sites to nest them, resulting in strong MSI [38]. Mawdsley et al. [39] demonstrated that strong MSI is conducive to forming transient Ni-containing surface phases such as La_2NiO_{4-y} adjacent to $LaFeO_3$, which could perform as a provisional medium to carry Ni atoms into and out of the perovskite lattice. Moreover, the bulk defects resulted from Sr and Co incorporation, as evidenced by TPR results, could form channels for Ni diffusion, and the high bulk oxygen mobility contributes to the process of driving oxygen atoms from air back to perovskite oxygen vacancies via the Mars-van Krevelen redox cycle mechanism.

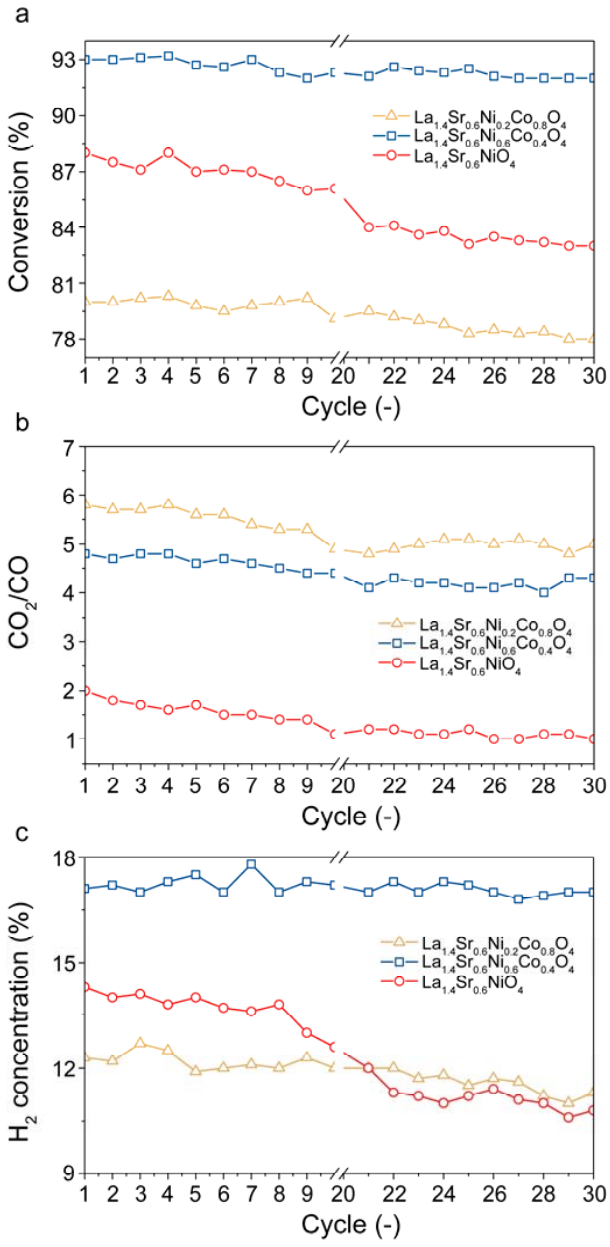

Figure 7. (**a**) Ethanol conversion, (**b**) CO_2/CO and (**c**) H_2 concentration during stability tests.

In conclusion, the CO_2/CO ratios for all the samples showed moderate decrease after the tests. $La_{1.4}Sr_{0.6}Ni_{0.2}Co_{0.8}O_4$ possessed the highest average ratio of 5.4 during the stability test due to the strong WGS capability of Co promotion. The average ethanol conversion of $La_{1.4}Sr_{0.6}Ni_{0.6}Co_{0.4}O_4$ (94.5%) was highest among three samples. $La_{1.4}Sr_{0.6}Ni_{0.6}Co_{0.4}O_4$ exhibited highest average H_2 concentration (17.2%) throughout the 50-cycle stability test due to the improved C–C rupture capability and tuning WGS activity. Meanwhile, $La_{1.4}Sr_{0.6}Ni_{0.6}Co_{0.4}O_4$ showed the highest stability, and the H_2 concentration of $La_{1.4}Sr_{0.6}Ni_{0.6}Co_{0.4}O_4$ decreased by about 0.3% at the end of the stability test. The improved stability of $La_{1.4}Sr_{0.6}Ni_{0.6}Co_{0.4}O_4$ is related to its having the strongest self-regeneration capability among three samples.

3. Materials and Methods

3.1. Preparation of OCs

A nickel-based perovskite structure OC was synthesized by the co-precipitation technique. Stoichiometric amounts of $Ni(NO_3)_2{\cdot}6H_2O$ (GR, 99%, Aladdin, Shanghai, China), $La(NO_3)_3{\cdot}6H_2O$ (AR, 99%, Aladdin, Shanghai, China), $Sr(NO_3)_2$ (99.97%, Aladdin, Shanghai, China) and $Co(NO_3)_2{\cdot}6H_2O$ (99.99%, Aladdin, Shanghai, China) were dissolved in deionized water under stirring. Then, ammonia of 1M was added dropwise to the solution under stirring at 50 °C, and maintaining a pH of about 8.5. Once the precipitation began to form, continuous stirring was carried out at 50 °C for one hour. Subsequently, the suspension was aged, filtrated and washed repeatedly until the pH was near neutral. After that, it was dried at 110 °C for about 15 h and calcined at 900 °C for 5 h. Finally, the fresh OCs were ground to 0.20–0.45 in diameter. The samples were denoted as $La_{1.4}Sr_{0.6}Ni_{1-x}Co_xO_4$ (x = 0, 0.4 and 0.8) after the loading of Co.

3.2. Characterization of OCs

XRD (Shimadzu XRD-6000 powder diffractometer, Kyoto, Japan) was used to identify the crystal phases of fresh and reduced OCs, where Cu Kα radiation (λ = 1.5406 Å) served as the X-ray source. TEM (FEI Tecnai G2, Hillsboro, OR, USA) was employed to investigate the morphology of the reduced OCs. The samples were ground and applied on a Cu grid coated with carbon film. H_2-TPR (Quantachrome OBP-1, Boynto Beach, FL, USA) was applied to ascertain the interaction of the fresh metal-support OCs. The samples were first heated at 450 °C in a He flow and then cooled at 90 °C. Subsequently, a flow of 10% H_2 in He was introduced at 20 mL/min. Meanwhile, the temperature increased to 800 °C at 10 °C/min. ICP-OES was employed to analyze the accurate elemental composition of the OCs. Prior to measurements, the samples were processed with the HNO_3 to remove Ni species on surface.

3.3. Activity and Stability Tests

The setup of our experimental system was described in our previous publications [17–19]. A mixture of OC of 1 g and quartz sand was loaded into a quartz tubular reactor (Φ15 × 800 mm). During the fuel feed step, a mixture of steam and ethanol with a steam to carbon (S/C) ratio of 3 was introduced into the reactor in a N_2 flow (300 mL/min). In the air feed step, an air flow of 600 mL/min was fed to eliminate carbon deposition and regenerate the OCs at 600 °C. The oxidation reactions ended when the oxygen concentration went back to ca. 21 vol%.

The ethanol conversion and steam conversion were calculated in the following equations:

$$X_{et} = \frac{\dot{n}_{et,in} - \dot{n}_{et,out}}{\dot{n}_{et,in}} \times 100\% \quad (1)$$

$$X_{H_2O} = \frac{X_{H_2O,in} - X_{H_2O,out}}{X_{H_2O,in}} \times 100\% \quad (2)$$

where $\dot{n}$ indicates the relevant molar flows (mol min^{-1}).

4. Conclusions

A series of $La_{1.4}Sr_{0.6}Ni_{1-x}Co_xO_4$ perovskite OCs for hydrogen production by employing Co and Ni as the B-site components of perovskite were synthesized. The synergistic effect between Ni and Co, which is beneficial to enhancing the catalytic activity and improve the stability of perovskite OCs, was investigated. $La_{1.4}Sr_{0.6}Ni_{0.6}Co_{0.4}O_4$ showed an average ethanol conversion of 92.4% and an average CO_2/CO ratio of 5.4 in a 30-cycle stability test. The Co doping was able to significantly improve the self-regeneration capability due to the increase in the number of oxygen vacancies in the perovskite lattice, therefore enhancing the sintering resistance. Moreover, the Co promotion also contributes to the improved WGS activity.

Author Contributions: Experiment, L.L., Q.Z., D.L. and Z.S.; Data Curation, B.J., Q.Z. and Z.S.; Writing-Original Draft Preparation, L.L. and B.J.; Writing-Review & Editing, L.L. and B.J.; Supervision, D.T. and L.L.; Project Administration, D.T. and L.L.; Funding Acquisition, L.L. and D.T.

Funding: This research was funded by [National Natural Science Foundation of China] grant number [51706030], [Fundamental Research Funds for Central Universities] grant number [DUT18JC11] and [China Postdoctoral Science Foundation] grant number [2017M611219].

Acknowledgments: We deeply appreciate the kind assistance from the Key Laboratory of Ocean Energy Utilization and Energy Conservation of Ministry of Education (China).

Conflicts of Interest: The authors declare no conflict of interest. The founding sponsors had no role in the design of the study; in the collection, analyses, or interpretation of data; in the writing of the manuscript, and in the decision to publish the results.

References

1. Wu, G.; Zhang, C.; Li, S.; Huang, Z.; Yan, S.; Wang, S.; Ma, X.; Gong, J. Sorption enhanced steam reforming of ethanol on Ni-CaO-Al_2O_3 multifunctional catalysts derived from hydrotalcite-like compounds. *Energy Environ. Sci.* **2012**, *5*, 8942–8949. [CrossRef]
2. Wang, C.; Chen, Y.; Cheng, Z.; Luo, X.; Jia, L.; Song, M.; Jiang, B.; Dou, B. Sorption-enhanced steam reforming of glycerol for hydrogen production over a NiO/$NiAl_2O_4$ Catalyst and Li_2ZrO_3-Based Sorbent. *Energy Fuel* **2015**, *29*, 7408–7418. [CrossRef]
3. Dou, B.; Zhang, H.; Cui, G.; Wang, Z.; Jiang, B.; Wang, K.; Chen, H.; Xu, Y. Hydrogen production by sorption-enhanced chemical looping steam reforming of ethanol in an alternating fixed-bed reactor: Sorbent to catalyst ratio dependencies. *Energy Convers. Manag.* **2018**, *155*, 243–252. [CrossRef]
4. Li, L.; Song, Y.; Jiang, B.; Wang, K.; Zhang, Q. A novel oxygen carrier for chemical looping reforming: $LaNiO_3$ perovskite supported on montmorillonite. *Energy* **2017**, *131*, 58–66. [CrossRef]
5. Wang, K.; Dou, B.; Jiang, B.; Song, Y.; Zhang, C.; Zhang, Q.; Chen, H.; Xu, Y. Renewable hydrogen production from chemical looping steam reforming of ethanol using *x*CeNi/SBA-15 oxygen carriers in a fixed-bed reactor. *Int. J. Hydrog. Energy* **2016**, *41*, 12899–12909. [CrossRef]
6. Jiang, B.; Li, L.; Bian, Z.; Li, Z.; Othman, M.; Sun, Z.; Tang, D.; Kawi, S.; Dou, B. Hydrogen generation from chemical looping reforming of glycerol by Ce-doped nickel phyllosilicate nanotube oxygen carriers. *Fuel* **2018**, *222*, 185–192. [CrossRef]
7. Tang, M.; Xu, L.; Fan, M. Progress in oxygen carrier development of methane-based chemical-looping reforming: A review. *Appl. Energy* **2015**, *151*, 143–156. [CrossRef]
8. Li, L.; Tang, D.; Song, Y.; Jiang, B.; Zhang, Q. Hydrogen production from ethanol steam reforming on Ni-Ce/MMT catalysts. *Energy* **2018**, *149*, 937–943. [CrossRef]
9. Jiang, B.; Zhang, C.; Wang, K.; Dou, B.; Song, Y.; Chen, H.; Xu, Y. Highly dispersed Ni/montmorillonite catalyst for glycerol steam reforming: Effect of Ni loading and calcination temperature. *Appl. Therm. Eng.* **2016**, *109*, 99–108. [CrossRef]
10. Li, L.; Jiang, B.; Tang, D.; Zhang, Q.; Zheng, Z. Hydrogen generation by acetic acid steam reforming over Ni-based catalysts derived from $La_{1-x}Ce_xNiO_3$ perovskite. *Int. J. Hydrog. Energy* **2018**, *43*, 6795–6803. [CrossRef]

11. Zhang, Q.; Li, L.; Jiang, B.; Wang, K.; Tang, D.; Dou, B. An intelligent oxygen carrier of $La_{2-x}Sr_xNiO_{4-\lambda}$ for hydrogen production by chemical looping reforming of ethanol. *Int. J. Hydrog. Energy* **2017**, *42*, 17102–17111. [CrossRef]
12. Nishihata, Y.; Mizuki, J.; Akao, T.; Tanaka, H.; Uenishi, M.; Kimura, M.; Okamoto, T.; Hamada, N. Self-regeneration of a Pd-perovskite catalyst for automotive emissions control. *Nature* **2002**, *418*, 164–167. [CrossRef] [PubMed]
13. Barbero, B.P.; Gamboa, J.A.; Cadús, L.E. Synthesis and characterisation of $La_{1-x}Ca_xFeO_3$ perovskite-type oxide catalysts for total oxidation of volatile organic compounds. *Appl. Catal. B* **2006**, *65*, 21–30. [CrossRef]
14. Maneerung, T.; Hidajat, K.; Kawi, S. $LaNiO_3$ perovskite catalyst precursor for rapid decomposition of methane: Influence of temperature and presence of H_2 in feed stream. *Catal. Today* **2011**, *171*, 24–35. [CrossRef]
15. Morales, M.; Segarra, M. Steam reforming and oxidative steam reforming of ethanol over $La_{0.6}Sr_{0.4}CoO_{3-\delta}$ perovskite as catalyst precursor for hydrogen production. *Appl. Catal. A* **2015**, *502*, 305–311. [CrossRef]
16. Wu, G.; Li, S.; Zhang, C.; Wang, T.; Gong, J. Glycerol steam reforming over perovskite-derived nickel-based catalysts. *Appl. Catal. B* **2014**, *144*, 277–285. [CrossRef]
17. Dou, B.; Zhang, H.; Cui, G.; Wang, Z.; Jiang, B.; Wang, K.; Chen, H.; Xu, Y. Hydrogen production and reduction of Ni-based oxygen carriers during chemical looping steam reforming of ethanol in a fixed-bed reactor. *Int. J. Hydrog. Energy* **2017**, *42*, 26217–26230. [CrossRef]
18. Jiang, B.; Dou, B.; Wang, K.; Zhang, C.; Li, M.; Chen, H.; Xu, Y. Sorption enhanced steam reforming of biodiesel by-product glycerol on Ni-CaO-MMT multifunctional catalysts. *Chem. Eng. J.* **2017**, *313*, 207–216. [CrossRef]
19. Ni, Y.; Wang, C.; Chen, Y.; Cai, X.; Dou, B.; Chen, H.; Xu, Y.; Jiang, B.; Wang, K. High purity hydrogen production from sorption enhanced chemical looping glycerol reforming: Application of NiO-based oxygen transfer materials and potassium promoted Li_2ZrO_3 as CO_2 sorbent. *Appl. Therm. Eng.* **2017**, *124*, 454–465. [CrossRef]
20. Lim, H.S.; Kang, D.; Lee, J.W. Phase transition of Fe_2O_3–NiO to $NiFe_2O_4$ in perovskite catalytic particles for enhanced methane chemical looping reforming-decomposition with CO_2 conversion. *Appl. Catal. B* **2017**, *202*, 175–183. [CrossRef]
21. Zhao, L.; Han, T.; Wang, H.; Zhang, L.; Liu, Y. Ni-Co alloy catalyst from $LaNi_{1-x}Co_xO_3$ perovskite supported on zirconia for steam reforming of ethanol. *Appl. Catal. B* **2016**, *187*, 19–29. [CrossRef]
22. Ma, H.; Zeng, L.; Tian, H.; Li, D.; Wang, X.; Li, X.; Gong, J. Efficient hydrogen production from ethanol steam reforming over La-modified ordered mesoporous Ni-based catalysts. *Appl. Catal. B* **2016**, *181*, 321–331. [CrossRef]
23. Taihei, N.; Motohiko, M.; Makoto, M. The Valence Control and Catalytic Properties of $La_{2-x}Sr_xNiO_4$. *Bull. Chem. Soc. Jpn.* **1988**, *61*, 3831–3837.
24. Nakamura, T.; Misono, M.; Yoneda, Y. Reduction-oxidation and catalytic properties of $La_{1-x}Sr_xCoO_3$. *J. Catal.* **1983**, *83*, 151–159. [CrossRef]
25. Takanabe, K.; Nagaoka, K.; Nariai, K.; Aika, K.-I. Titania-supported cobalt and nickel bimetallic catalysts for carbon dioxide reforming of methane. *J. Catal.* **2005**, *232*, 268–275. [CrossRef]
26. Valderrama, G.; Goldwasser, M.R.; de Navarro, C.U.; Tatibouët, J.M.; Barrault, J.; Batiot-Dupeyrat, C.; Martinez, F. Dry reforming of methane over Ni perovskite type oxides. *Catal. Today* **2005**, *107–108*, 785–791. [CrossRef]
27. Müller, C.A.; Maciejewski, M.; Koeppel, R.A.; Baiker, A. Combustion of Methane over Palladium/Zirconia Derived from a Glassy Pd–Zr Alloy: Effect of Pd Particle Size on Catalytic Behavior. *J. Catal.* **1997**, *166*, 36–43. [CrossRef]
28. Valderrama, G.; Kiennemann, A.; Goldwasser, M.R. La-Sr-Ni-Co-O based perovskite-type solid solutions as catalyst precursors in the CO_2 reforming of methane. *J. Power Sources* **2010**, *195*, 1765–1771. [CrossRef]
29. Jiang, B.; Dou, B.; Song, Y.; Zhang, C.; Du, B.; Chen, H.; Wang, C.; Xu, Y. Hydrogen production from chemical looping steam reforming of glycerol by Ni-based oxygen carrier in a fixed-bed reactor. *Chem. Eng. J.* **2015**, *280*, 459–467. [CrossRef]
30. Jiang, B.; Dou, B.; Wang, K.; Zhang, C.; Song, Y.; Chen, H.; Xu, Y. Hydrogen production by chemical looping steam reforming of ethanol using NiO/montmorillonite oxygen carriers in a fixed-bed reactor. *Chem. Eng. J.* **2016**, *298*, 96–106. [CrossRef]

31. Hossain, M.M.; de Lasa, H.I. Reactivity and stability of Co-Ni/Al_2O_3 oxygen carrier in multicycle CLC. *AIChE J.* **2007**, *53*, 1817–1829. [CrossRef]
32. Li, D.; Li, X.; Gong, J. Catalytic reforming of oxygenates: State of the art and future prospects. *Chem. Rev.* **2016**, *116*, 11529–11653. [CrossRef] [PubMed]
33. Sinfelt, J.H.; Yates, D.J.C. Catalytic hydrogenolysis of ethane over the noble metals of Group VIII. *J. Catal.* **1967**, *8*, 82–90. [CrossRef]
34. Hu, X.; Lu, G. Investigation of steam reforming of acetic acid to hydrogen over Ni–Co metal catalyst. *J. Mol. Catal. A Chem.* **2007**, *261*, 43–48. [CrossRef]
35. Shafiefarhood, A.; Galinsky, N.; Huang, Y.; Chen, Y.; Li, F. Fe_2O_3@$La_xSr_{1-x}FeO_3$ core–shell redox catalyst for methane partial oxidation. *ChemCatChem* **2014**, *6*, 790–799. [CrossRef]
36. Chen, D.; Christensen, K.O.; Ochoa-Fernández, E.; Yu, Z.; Tøtdal, B.; Latorre, N.; Monzón, A.; Holmen, A. Synthesis of carbon nanofibers: Effects of Ni crystal size during methane decomposition. *J. Catal.* **2005**, *229*, 82–96. [CrossRef]
37. Mei, D.; Lebarbier Dagle, V.; Xing, R.; Albrecht, K.O.; Dagle, R.A. Steam reforming of ethylene glycol over $MgAl_2O_4$ supported Rh, Ni, and Co catalysts. *ACS Catal.* **2016**, *6*, 315–325. [CrossRef]
38. Deng, J.; Cai, M.; Sun, W.; Liao, X.; Chu, W.; Zhao, X.S. Oxidative methane reforming with an intelligent catalyst: Sintering-tolerant supported nickel nanoparticles. *ChemSusChem* **2013**, *6*, 2061–2065. [CrossRef] [PubMed]
39. Mawdsley, J.R.; Vaughey, J.T.; Krause, T.R. Neutron diffraction studies of nickel-containing perovskite oxide catalysts exposed to autothermal reforming environments. *Chem. Mater.* **2009**, *21*, 4830–4838. [CrossRef]